Modeling the hygrothermal behavior of green walls in Comsol Multiphysics® : validation against measurements in a climate chamber

Reference:
Alvarado Alvarado Allan Augusto, De Bock Anouk, Ysebaert Tess, Belmans Bert, Denys Siegfried.- Modeling the hygrothermal behavior of green walls in Comsol Multiphysics® : validation against measurements in a climate chamber
Building and environment - ISSN 1873-684X - 238(2023), 110377
Full text (Publisher's DOI): https://doi.org/10.1016/J.BUILDENV.2023.110377
To cite this reference: https://hdl.handle.net/10067/1964670151162165141

Modeling the hygrothermal behavior of green walls in Comsol Multiphysics®: Validation against measurements in a climate chamber

Allan A. Alvarado-Alvarado[1], Anouk De Bock[2], Tess Ysebaert[1], Bert Belmans[2,3], Siegfried Denys[1,*]

[1]Sustainable Energy, Air and Water Technology (DuEL), Department of Bioscience Engineering, University of Antwerp, Groenenborgerlaan 171 2020 Antwerp, Belgium

[2]Energy and Materials in Infrastructure and Buildings (EMIB), Department of Applied Engineering, University of Antwerp, Groenenborgerlaan 171 2020 Antwerp, Belgium

[3]Vrije Universiteit Brussel, Department of Architectural Engineering, Architectural Engineering Research Group, Pleinlaan 2, B-1050 Brussel, Belgium

[*]Corresponding author: Siegfried Denys

Email: Siegfried.Denys@uantwerpen.be

Full postal address: Groenenborgerlaan 171, 2020 Antwerpen, Belgium

Abstract

Green walls (GW) can diminish building's surface temperature through shading, insulation, and evapotranspiration mechanisms. These can be analyzed by computer models that account for heat and mass transfer phenomena. However, most previous models were one-dimensional thermal simulations in which boundary conditions (BC), like convective moisture transport, were not or only partly considered. The present work proposes a more comprehensive way to predict GW's hygrothermal behavior by integrating a 3D multiphysics model that couples heat and moisture transport in Comsol Multiphysics®. The air cavity that usually separates the GW from the building was also considered. Heat sink terms were added to represent plants' transpiration and substrates' evaporation, considering the leaf area density (LAD) and substrate's water saturation (Sr). The model was validated against experiments where four green wall-test panels (GW-TPs) were evaluated in a climate chamber under steady-state conditions. This provides a much sounder approach for validation than what currently exists (r = 0.97; RMSE = 0.33 °C). The four GW-TPs decreased the masonry's surface temperature in the range of 0.89 to 1.14 ˚C (0.97 ± 0.11 SD ˚C). The average contribution of the evapotranspiration effect was 30%, whereas the contribution of the air cavity was 60.7 ± 0.09 %. The temperature at the substrate's rear was reduced on average by 0.57 ± 0.15 SD °C. When solar radiation was considered as a BC, the GW-TPs decreased the building's surface temperature by 10˚C. Lastly, high values of LAD and Sr translated into increased temperature reduction values.

Keywords: evapotranspiration, green wall, heat transfer, hygrothermal behavior, mass transfer, multiphysics modeling.

	NOMENCLATURE	
BC	Boundary condition	(-)
$\boldsymbol{C}$	Concentration of moisture	kg m^{-3}
$\boldsymbol{C_p}$	Heat capacity at constant pressure	*J kg^{-1} K^{-1}*
$\boldsymbol{c_0}$	Empirical coefficient	(-)
$\boldsymbol{c_1}$	Empirical coefficient	(-)
$\boldsymbol{c_2}$	Empirical coefficient	(-)
$\boldsymbol{D}$	Vapor diffusion coefficient of air	m^2 s^{-1}
$\boldsymbol{d_0}$	Displacement height	(-)
$\boldsymbol{ET_o}$	Evapotranspiration of reference	mm day^{-1}
$\boldsymbol{F}$	Volume force	N m^{-3}
$\boldsymbol{G}$	Global moisture source	kg m^{-3} s^{-1}
$\boldsymbol{g}$	Gravity	m s^{-2}
$\boldsymbol{g_w}$	Moisture vector flux	kg m^{-2} s^{-1}
GW	Green wall	(-)
GW-TP	Green wall-test PANEL(s)	(-)
$\boldsymbol{h_{ht}}$	Heat transfer coefficient	*W m^{-2} K^{-1}*
$\boldsymbol{h_m}$	Mass transfer coefficient	*m s^{-1}*
$\boldsymbol{k}$	Thermal conductivity	*W m^{-1} K^{-1}*
$\boldsymbol{K_c}$	Active leaf area coefficient	(-)
$\boldsymbol{L}$	Plate length	m
$\boldsymbol{LAD}$	Leaf area density	m^2 m^{-3}
$\boldsymbol{m}$	Mass vector flux	kg m^{-2} s^{-1}
$\boldsymbol{p}$	Vapor pressure	Pa
$\boldsymbol{Q}$	Global heat source	W m^{-3}
$\boldsymbol{Q_{trans}}$	Heat sink transpiration (vegetation)	W m^{-3}
$\boldsymbol{Q_{ev}}$	Heat sink evaporation (substrate)	W m^{-3}
$\boldsymbol{q}$	Heat vector flux	W m^{-2}
$\boldsymbol{r_a}$	Aerodynamic resistance	s m^{-1}
$\boldsymbol{Ra_L}$	Rayleigh number	(-)
RH	Relative humidity	(%)
$\boldsymbol{r_s}$	Stomatal resistance	s m^{-1}
$\boldsymbol{r_{sub}}$	Resistance to vapor transfer	s m^{-1}
$\boldsymbol{Sr}$	Substrate's water saturation	m^{-3} m^{-3}
$\boldsymbol{T}$	Temperature	K
$\boldsymbol{u}$	Wind speed	m s^{-1}
$\boldsymbol{w}$	Water content	kg m^{-3}
$\boldsymbol{y}$	Vegetation thickness	m
$\boldsymbol{z}$	Wind speed altitude measurements	(-)
$\boldsymbol{z_{om}}$	Roughness length	(-)
	GREEK SYMBOLS	
$\boldsymbol{\Delta}$	Slope of the saturated vapor pressure curve	kPa K^{-1}
$\boldsymbol{\alpha_V}$	Volumetric coefficient of thermal expansion	(-)
$\boldsymbol{\delta}$	Vapor permeability of still air	s
$\boldsymbol{\delta_p}$	Vapor permeability	s
$\boldsymbol{\phi_w}$	Relative humidity	(-)
$\boldsymbol{\gamma}$	Thermodynamic psychometric constant	Pa K^{-1}
$\boldsymbol{\kappa}$	Von Karman's constant	(-)
$\boldsymbol{\eta}$	Dynamic viscosity	Pa s
$\boldsymbol{\mu}$	Vapor resistance factor	(-)
$\boldsymbol{\rho}$	Density	kg m^{-3}
	SUBSCRIPTS	
$\boldsymbol{a}$	Aerodynamic	
$\boldsymbol{air}$	Air	
$\boldsymbol{conv}$	Convective	
$\boldsymbol{eff}$	Effective	
$\boldsymbol{ext}$	Exterior	
$\boldsymbol{gb}$	Rear substrate	
$\boldsymbol{ht}$	Heat transfer	
$\boldsymbol{int}$	Interior	
$\boldsymbol{m}$	Mass transfer	
$\boldsymbol{ref}$	Reference	
$\boldsymbol{s}$	Stomatal	
$\boldsymbol{sat}$	Saturation	
$\boldsymbol{solid}$	Solid	
$\boldsymbol{sub}$	Of the substrate	
$\boldsymbol{surf}$	Surface	
$\boldsymbol{w}$	Outer masonry's surface	

1. Introduction

1.1 Green walls and urban heat island effect

Rapid urbanization has caused urban heat islands (UHI) to become a common problem in cities worldwide. As a result, higher urban temperatures lead to discomfort, impact human health, and increase energy consumption for cooling (Koch *et al.,* 2020). Increasing the amount of vegetation in cities has proven to be an effective mitigation measure to reduce the UHI effect. Green walls (GW) are a kind of urban vegetation technology that may be used for this purpose. They can be classified based on the growing type into "green faces or vegetated coverings" (GF) and "living wall systems" (LWS) (van de Wouw, Ros and Brouwers, 2017). GF and LWS have been researched at different scales (Malys, Musy and Inard, 2014).

The associated benefits of GW include energy savings, urban microclimate regulation, sound attenuation, air purification, and social and psychological aspects (Djedjig *et al.,* 2017). Several studies have demonstrated that green walls can decrease the indoor temperature from 0.5 to 7 °C, depending on the type of green wall and preconditions such as orientation (Malys, Musy and Inard, 2014). The thermal behavior of GW has been described as very sensitive to the climatic context, characteristics of the green coating, and operational configuration. Consequently, thermal effects are often the focus of green wall studies, which are investigated by comparing the building wall's temperature with and without a vegetated envelope. The thermal behavior of a GW will significantly differ from common construction materials, given that they consist of living materials like plants. In addition, a substrate layer also modifies the thermal behavior, and it serves as attachment and nutrition (Djedjig et al., 2017a).

1.2 Hygrothermal benefits of green walls

GW's benefits can be investigated from a hygrothermal viewpoint, i.e., heat and moisture transfer, by accounting for the most influential phenomena through its different layers. Three main mechanisms are usually considered: shading, insulation, and evapotranspiration (Djedjig *et al.*, 2012). The first relates to solar radiation, as plants reflect part of the incoming solar radiation depending on their characteristics, transmitting only a fraction to the next layer. Insulation refers to the thermal resistance to heat transfer through the GW's layers, and empirical relations have been developed to calculate heat transfer coefficients between the GW and surroundings (Fabiana Convertino, Vox and Schettini, 2019). Plants have a specific heat capacity similar to that of water but a lower thermal conductivity and can therefore act as efficient heat sinks (Jayalakshmy and Philip, 2010). In addition, an air cavity usually exists between the GW and the building, which can offer additional insulation if poorly ventilated (Convertino, Vox and Schettini, 2021).

Research has shown that the most challenging task is analyzing the evapotranspiration effect due to the dynamic behavior of plants. Seasonal and growth cycles and changes in the substrate's moisture contribute to GW's changing aspects. Therefore, modeling evapotranspiration is likewise challenging yet relevant as it is recognized as a cooling tool. Plants consume 2.45 MJ/kg of latent heat to vaporize water which cools the surroundings adiabatically (van de Wouw, Ros and Brouwers, 2017). Hence, plants act as heat sinks, and the more latent heat they consume translates into more cooling. Plant growth cycle and characteristics, substrate properties, and weather conditions determine evapotranspiration (van de Wouw, Ros and Brouwers, 2017).

Traditionally, the thermal modeling of GW involves a heat transfer analysis in which the general heat conduction equation is employed (Šuklje, Medved and Arkar, 2016; Widiastuti et al., 2022). Since this is a partial differential equation, boundary conditions corresponding to the outdoor and indoor environment are used to achieve a solution. Frequently, a steady-state calculation is adopted, neglecting transient effects (Carlini et al., 2014). Nevertheless, the reality is more complex since outdoor and indoor conditions are transient. The latter implies that high interest in analyzing time-dependent hygrothermal behavior. On the other hand, hygrothermal models have been scarcely developed in which moisture transport is considered (**Table 1**). Previous thermal and hygrothermal models of GW adapt equations from green roof models using balances applied to the external and internal faces of the GW(Malys, Musy and Inard, 2014).

Table 1. Recent thermal and hygrothermal models of green walls in buildings: their scope and considered mechanisms.

Authors/Year	**Software Integration**	**Model's scope**		***Green walls' benefits simulated***			**Indoor conditions**
		Thermal	*Hygro-thermal*	*Shading*	*Insulation*	*Evapo-transpiration*	
(Arenghi, Perra and Caffi, 2021)	EnergyPlus	✓		*YES*	*YES*	*YES*	NO
(Freewan, Jaradat and Amaireh, 2022)	DesignBuilder	✓		*YES*	*YES*	*YES*	NO
(Zhang, Zhang and Meng, 2022)	EnergyPlus	✓		*YES*	*YES*	*YES*	NO
(Kenai *et al.*, 2021)	TRNSYS	✓		*YES*	*YES*	*NO*	YES
(Škerget, Tadeu and Almeida, 2021)	Finite Difference Method (FDM)		✓	*YES*	*YES*	*YES*	YES
(Hoffmann *et al.*, 2021)	R		✓	*YES*	*YES*	*YES*	YES

1.3 Objectives and scope of the study

As seen in **Table 1**, previous work on GW modeling has primarily been thermal-based, employing a one-dimensional nodal approach. These models have been integrated into common Building Energy Simulation software like TRNSYS and EnergyPlus (Djedjig, Bozonnet and Belarbi, 2016; Arenghi, Perra and Caffi, 2021). The nodal approach requires fewer calculations, as meshing is not necessary. Nevertheless, it treats each zone as a homogenous volume with uniform physical variables. For instance, the temperature distribution is not obtained within a volume (Hamdaoui *et al.*, 2021).

Certainly, thermal models of GW have neglected the convective moisture transfer (which affects heat transfer) occurring at the external surface of the GW's vegetation, i.e., exterior, and the internal surface of the building's, i.e., interior. Therefore, both heat and moisture transfer phenomena must be coupled in a hygrothermal model of GW to approximate reality. For this purpose, the vapor resistance factor must be considered as it determines the moisture transfer.

The present study aims to model the hygrothermal behavior of green walls (GW) mounted on the external surface of buildings by integrating and coupling heat and moisture balance equations into a three-dimensional (3D) multiphysics model. The software package Comsol Multiphysics® is utilized for GW for the first time. The CFD approach provides a detailed analysis of the various fluxes occurring inside and outside buildings, which is desired for a hygrothermal model of a GW. Yet it takes more time to converge to a solution than a nodal approach; it provides detailed information on the temperature field at all points in space (Hamdaoui *et al.*, 2021). Therefore, the 3D geometry was chosen to better represent a GW's real dimensions and apply more boundary conditions.

Additionally, a 3D geometry offers the advantage of modeling the air cavity between the GW and the building wall and calculating its contribution to the reduction in temperature at the building's wall surface. Additional sink heat terms for the transpiration (plants) and evaporation (substrate) mechanisms are introduced to account for the evapotranspiration effect of a GW. Two key parameters of a GW were varied to analyze the effect on temperature reduction, namely leaf area density ($\boldsymbol{LAD}$) and substrate's water saturation ($\boldsymbol{Sr}$). The model output was validated against experimental data from four commercial green wall-test panels (GW-TPs) evaluated in a climate chamber.

2 Experiments in a climate chamber

2.1 Green wall-test panels

Four commercial green wall-test panels (GW-TP) or segments of actual green walls (**Appendix A**) consisting of two compartments, (i) vegetation and (ii) substrate, were evaluated in a climate chamber. Each GW-TP contained a different substrate and the same combination of plant species. An overview of the GW-TP and the CW construction is shown in **Table 2**.

Table 2.Geometry of the setup reproduced in the climate chamber with a 6 cm-air cavity between the green wall-test panel (GW-TP) and the outer leaf of the insulated cavity wall (CW).

Section	Layer	Green wall-test panel (GW-TP)	Thickness (m)	Composition
1. Green wall (GW)	Vegetation	All	0.05	*Bergenia cardifolia, Carex morrowii, Vinca minor, Lonicera nítida, Iberis sempervirens, Lavandula angustifolia* (randomly planted)
	Substrate	A	0.10	Rockwool
		B	0.05	Rockwool
		C	0.10	Potting soil
		D	0.10	Peatmoss
2. Air cavity (AC)	Air	-	0.06	-
3. Insulated air cavity wall (CW)	Masonry	-	0.10	-
	Air		0.03	
	Rockwool		0.05	
	Thermobrick		0.09	

2.2 Climate chamber

A modular two-zone climate chamber was used to evaluate the GW-TP (**Appendix B**). The climate chamber allows recreating outdoor and indoor conditions on both sides of a green wall-test panel (GW-TP) by stationary or dynamic input of temperature and relative humidity. These settings were used as boundary conditions in the hygrothermal model (**section 3.3**). The climate chamber applied stationary temperature and relative humidity setpoints to reproduce conditions of a typical summer day in Belgium at noon (exterior = 24˚C T, 55% RH; interior: 21˚C T, 45% RH). Notably, solar radiation was not reproduced in the climate chamber due to the absence of an artificial sun.

An air cavity exists between the backside of the green wall-test panel (GW-TP) and the outer leaf of the insulated cavity wall (CW), i.e., the masonry's surface. For all GW-TPs, the air cavity was enclosed to avoid intense mixing with the air in the room to mimic the real conditions behind a large continuous green wall. A cavity distance of 6 cm was maintained for all the evaluated GW-TPs. Furthermore, sensors to monitor temperature (T1-T6) (FPA22L0100 ALMEMO® ± 0.2 K) and relative humidity (RH1-RH6) (FHAD4641L05 ALMEMO® ± 3%). They were purposefully installed across the setup in three regions of interest: (i) in the middle of the vegetation, (ii) on the backside of the substrate, and (iii) at various depths in the construction of the insulated cavity wall (CW). Sensors were also installed in the exterior and interior rooms of the chamber (**Appendix B**). Therefore, temperature and relative humidity profiles across the setup could be obtained to be contrasted against the hygrothermal model.

3 Hygrothermal model

3.1 Geometry

The geometry was first defined to build the model in Comsol Multiphysics®. The model's geometry replicated the green wall section (GW-TP) and the insulated cavity wall (CW) installed in the climate chamber (**Table 2**). Then, a mesh convergence study was performed considering five meshing options. The comparison was based on the model's output, i.e., temperature profiles throughout the geometry, from which datasets containing the points were obtained. A one-way ANOVA was carried out, resulting in a P-value > 0.05. Therefore, it was concluded that there was no difference among the meshes, and therefore, a normal mesh was used, given its low computational demand.

3.2 Model description

The hygrothermal model consisted of a steady-state study coupling heat and moisture transfer equations and heat sink terms. The governing equations and boundary conditions are shown in **Table 3**. Data from the external and internal sides of the geometry were included as boundary conditions (**section 2.2**), whereas the rest of the boundaries were adiabatic, i.e., thermally insulated. The vegetation and substrate layers of the GW-TP and the layers constituting the insulated cavity wall (CW) were modeled as homogeneous solid media. An exception was made for the air cavity, which was modeled as a fluid. Layers' thermophysical properties are shown in **Appendix C**. Transpiration and evaporation terms were modeled as uniform volumetric heat sinks. The model was integrated into the commercial software package Comsol Multiphysics® 6.0 using a computer with a 64-bit operating system and Intel ® Xeon ® CPU E5-1650 v3 @3.50 GHz and 128 GB of RAM.

Table 3. Summary of the hygrothermal model, including governing equations and boundary conditions. Elaborated from Djedjig et al. (2012, 2017); Cascione et al. (2017); van de Wouw, Ros and Brouwers (2017); Convertino, Vox and Schettini (2019).

PROCESS	No.	NAME	EQUATION	DESCRIPTION	UNITS
			A. Governing Equations		
Heat transfer balance	Eq. 1	Heat source	$\nabla \cdot q = Q - (Q_{trans} + Q_{evap})$	The heat of transpiration and evaporation is deducted from the global heat source.	W m^{-3}
	Eq. 2	Heat flow vector field	$q = -k_{eff} \nabla T$	Heat transfer depends on effective thermal conductivity.	W m^{-2}
	Eq. 3	Effective thermal conductivity	$k_{eff} = k_{solid}\left(1 + \frac{w(\phi_w)}{\rho_{solid}}\right)$	The effective thermal conductivity is affected by moisture transport.	W m^{-1} K^{-1}
Moisture transfer balance	Eq. 4	Moisture source	$\nabla \cdot g_w = G$	The global moisture source is the divergence of the moisture vector field.	kg m^{-3} s^{-1}
	Eq. 5	Moisture flow vector field	$g_w = -(\delta_p \nabla(\phi_w p_{sat}))$	Moisture transfer is given by the material's permeability and partial pressure of air.	kg m^{-2} s^{-1}
	Eq. 6	Material's vapor permeability	$\delta_p = \frac{\delta}{\mu}$	The vapor resistance factor gives the material air permeability.	s
			B. Boundary Conditions		
Convective heat transfer	Eq. 7	Convective heat flux	$q_{conv} = h_{ht,conv}(T_{surf} - T_{ext})$	Convective heat transfer depends on a heat transfer coefficient and a temperature gradient.	W m^{-2}
	Eq. 8	Convective heat transfer coefficient (exterior)	$h_{ht,conv,ext} = 5.9 + 4.1u\frac{511 + 294}{511 + T_{ext}}$	Empirical formulas describe the convective heat transfer coefficients at the exterior of a green wall and interior.	W m^{-2} K^{-1}
	Eq. 9	Convective heat transfer coefficient (interior)	$h_{ht,conv,int} = \frac{k}{L}\left(0.68 + \frac{0.67Ra_L^{\frac{1}{4}}}{\left(1 + \left(\frac{0.492k}{\eta C_p}\right)^{\frac{9}{16}}\right)^{\frac{4}{9}}}\right)$		W m^{-2} K^{-1}
Convective moisture transfer	Eq. 10	Convective moisture flux	$m_{conv} = h_{m,conv}(C_{surf} - C_{ext})$	Convective moisture transfer depends on a moisture transfer coefficient and a moisture gradient.	kg m^{-2} s^{-1}
	Eq. 11	Convective moisture transfer coefficient (exterior)	$h_{m,conv,ext} = \frac{D}{k}\left(\frac{k}{\rho C_p D}\right)^{1/3} * h_{ht,conv,ext}$	Empirical formulas describe the convective moisture transfer coefficients at the exterior of a green wall and interior.	m s^{-1}
	Eq. 12	Convective moisture transfer coefficient (interior)	$h_{m,conv,int} = \frac{D}{k}\left(\frac{k}{\rho C_p D}\right)^{1/3} * h_{ht,conv,int}$		m s^{-1}
Evapotranspiration (heat sink)	Eq. 13	Heat of transpiration-plants	$Q_{trans} = K_c LAD \frac{(\rho c_p)_{air}}{\gamma(r_a + r_s)}(p_{sat} - p_{air})$	Transpiration heat sink depends on leaf area, resistances, and a vapor pressure gradient.	W m^{-3}
	Eq. 14	Heat of evaporation - substrate	$Q_{evap} = \frac{(\rho c_p)_{air}}{\gamma(r_{sub})}(p_{sat} - p_{air})$	Evaporation (heat sink) depends on resistances and a vapor pressure gradient.	W m^{-3}

*In the hygrothermal model (**Table 3***

), **Eq. 1** and **Eq. *4*** show the global heat and moisture balances steady-state conditions. **Eq. 1** describes that the divergence of the heat flow vector field (q) equals the global heat source (Q) from which an amount of heat is deducted by the heat sink terms that correspond to vegetation's transpiration (Q_{trans}) and substrate's evaporation (Q_{ev}), calculated from **Eq. 13 Eq. 14** respectively. q is given by the effective thermal conductivity (k_{eff}) and the temperature gradient (∇T) (**Eq. 2**). The heat sink terms are introduced as user-defined volumetric heat sink terms and are further elaborated in **section 3.5**

The water content depends on relative humidity ($w(\phi_w)$) and affects q by producing a change in effective thermal conductivity (k_{eff}). The latter considers the material's dry solid thermal conductivity (k_{Solid}) and density (ρ_{solid}) (**Eq. 3**).

The global moisture source (G) in **Eq. *4*** is given by the divergence of the moisture transport field vector (g_w) (**Eq. *5***). The model considers vapor diffusion through materials depending on the vapor permeability (δ_p). The materials' vapor resistance factor (μ) was used instead of the vapor permeability (δ_p) and its conversion is automatically performed by considering the vapor permeability of still air (δ) (**Eq. *6***).

Natural convection occurring in the enclosed air cavity, i.e., between the green wall test panel (GW-TP) and the outer leaf of the insulated cavity wall, i.e., masonry's surface, was modeled. The air cavity was modeled using the Boussinesq approximation, which states that buoyancy occurs due to a variation in density expressed by temperature differences. A small change in density is accounted for in a volume force term. The latter term is introduced in the momentum equation in the opposite direction of gravity.

3.3 Boundary conditions

Convection is a common boundary condition when modeling heat and mass transfer, i.e., a fluid cools or heats a surface through natural or forced convection. Forced heat and mass convection are typically the prevailing convection type at the exterior of a green wall, i.e., vegetation's surface (Fabiana Convertino, Vox and Schettini, 2019). In contrast, natural heat and mass convection were assumed at the interior of the insulated cavity wall, i.e., the thermobrick surface. Adiabatic BC was used in the rest of the boundaries, i.e., no heat flux.

The forced heat and mass convection BC was introduced by applying a convective heat flux (q_{conv}) and a convective moisture flux (m_{conv}) at the vegetation surface (**Eq. *7* and Eq. *10***). These fluxes depend on the gradient between the bulk temperature (T_{ext}) and bulk moisture (C_{ext}) surrounding the surface and the same quantities at the surface (T_{surf}), (C_{surf}). Convective heat and moisture transfer coefficients are required for the calculation of the fluxes.

We employed the empirical relationship developed by Convertino, Vox and Schettini (2019) and Ayata, Tabares-Velasco and Srebric (2011) for the calculation of the convective heat transfer coefficient ($h_{ht,conv,ext}$) at the vegetation surface (**Eq. *8***). On the other hand, empirical relationships available in the software package were used to obtain the convective heat transfer coefficient at the interior ($h_{ht,conv,int}$) (**Eq. *9***), as well as for the moisture transfer coefficients at the vegetation surface ($h_{m,conv,ext}$) (**Eq. *11***) and interior ($h_{m,conv,int}$) (**Eq. *12*).** Moisture transfer coefficients calculation depend on the heat transfer coefficient. These relationships involve the Rayleigh number (Ra_L), plate length (L), bulk temperature (T_{ext}), thermal conductivity (k), dynamic viscosity (η), and the vapor diffusion coefficient of air (D).

3.4 Thermophysical properties

The relevant thermophysical properties in this study include density ($\boldsymbol{\rho}$), specific heat capacity ($\boldsymbol{C_p}$), thermal conductivity ($\boldsymbol{k}$), and a vapor resistance factor ($\boldsymbol{\mu}$), as shown in **Appendix C**. A literature review provided average values for the vegetation and substrate properties. Similarly, the properties of the materials constituting the insulated cavity wall (CW) were obtained from the manufacturer's data sheets.

3.5 Evapotranspiration

As stated above, the model elaborates and applies heat sink terms, i.e., the heat taken by transpiration (plants) and evaporation (substrate) that is subtracted from the global heat source (**Eq. 13 and Eq. 14**). The two heat sink terms represent the evapotranspiration effect corresponding to the conversion from sensible to latent heat.

3.6.1 Plants' transpiration

The transpiration heat sink term is an adaptation of the Penman-Monteith equation. This equation provides an ideal reference evapotranspiration value for "a hypothetical reference crop with an assumed crop height of 0.12 m, a fixed surface resistance of 70 s m$^{-1,}$ and an albedo of 0.23" (Widiastuti *et al.*, 2022). A modification of the Penman-Monteith equation is necessary to apply it in the hygrothermal model. For this purpose, the leaf area density of the vegetation compartment (LAD) is considered in the calculation of heat of transpiration (Q_{trans}) (**Eq. 13)**. LAD values of 0.5, 0.8, 0.6, and 1.0 for the PANEL's A, B, C, and D were visually approached based on the leaf area that covered the substrate. Nevertheless, not all the LAD is active, and hence, an active leaf area coefficient (K_c) was introduced, taking a mean value of 0.9 from previously used values to calculate the effect under adjusted conditions (ET-adj). K_c values ranging 0.1 to 1.7 were reported by Lazzara and Rana (2010) and van de Wouw, Ros and Brouwers, (2017).

Eq. 13 shows the calculation of the transpiration heat sink term, in which $(\rho c_p)_{air}$ represents the air volumetric heat capacity, γ is the thermodynamic psychometric constant, and r_a and r_s account for an aerodynamic and stomatal resistance to transpiration. p_{sat} is the saturation vapor pressure evaluated at leaf temperature, i.e., vegetation surface, while p_{air} is the vapor pressure of the surrounding bulk air (Arkebauer, 2005).

An aerodynamic resistance (r_a) to transpiration was estimated (23 s m^{-1}), expressed in terms of the wind speed (u) and empirical terms. On the other hand, the stomatal resistance to transpiration (r_s) is a purely biological parameter, and a mean value of 150 s m^{-1} was chosen, as reported by Sailor (2008).

3.6.2 Substrate's evaporation

The heat taken by the substrate's evaporation (Q_{ev}) **(Eq. 14)** is calculated by a difference in saturation vapor pressure, i.e., between the substrate's surface and the surrounding air. A resistance to vapor transfer (r_{sub}) was accounted for, which is given by the substrate's water saturation. An average value of 0.2 m^3 m^{-3} of a typical soil was chosen for all GW-TPs except PANEL D (0.4 m^3 m^{-3}), as the substrate (peat moss) can hold more water (Arenghi, Perra and Caffi, 2021).

4 Model validation

The model's accuracy was assessed using the Pearson correlation coefficient (r) and the root-mean-square error (RMSE). The correlation coefficient (r) describes the association between the predicted and the experimentally obtained values, whereas RMSE assesses the prediction accuracy. On the other hand, the overall evaluation of the benefits of the green walls was done by comparing the results between a bare wall case (section 0), i.e., only insulated air cavity wall, vs. a green wall case, i.e., with GW-TP (section 5.2).

5 Results and discussion

5.1 Bare wall scenario

The validation of the hygrothermal model under stationary conditions for the bare wall case, i.e., insulated cavity wall (CW), is shown in **Figure 1**. The bare wall scenario depicts the heat and moisture transfer through the different materials of the insulated cavity wall (CW). Temperature and relative humidity profiles across the insulated cavity wall (CW) were obtained from the model's output and plotted against experimental data from the sensors to validate their congruency. The masonry's surface temperature (T_w) evaluated in this case is the comparison basis for calculating the temperature reduction that the GW provide. A high agreement (r = 0.97) between the measured points and the model's output was observed for the variable temperature (**Figure 1**). In contrast, the same measure was lower for relative humidity. RMSE was significantly low for temperature (RSME = 0.33 °C) and relative humidity (RSME = 4.33 %), indicating a low error.

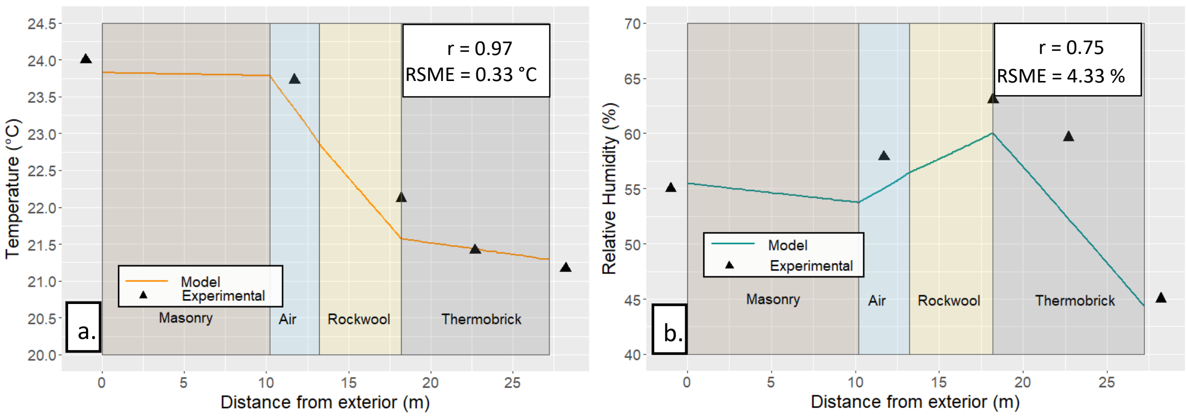

Figure 1. (a) Predicted temperature profile (model) and experimental measurements (triangles) from the insulted cavity wall (CW) that represents the bare wall scenario. (b) Predicted relative humidity profile (model) and experimental measurements (triangles) for the insulted air cavity wall (CW). Note: The first and the last measured points (outside geometry) in each figure represent the exterior and interior room temperature and relative humidity, i.e., setpoints in the climate chamber.

Figure 1 shows that the masonry provides poor insulation given its thermal conductivity (***k*** =1.61 W m^{-1} K^{-1}), which contrasts with the insulation of the internal air gap, i.e., between the masonry and the Rockwool. This air gap was assumed to be a stagnant layer of air (***k*** = 0.025

W m^{-1} K^{-1}), and natural convection was not modeled. Consequently, a steep decrease in the temperature profile can be seen in this section, which arises due to the high insulation provided by the next layer of Rockwool ($\boldsymbol{k}$ =0.035 W m^{-1} K^{-1}).

The hygrothermal model applied to the bare wall scenario predicted a temperature of 23.8 °C at the masonry's surface.. Notably, the temperature at this point was slightly below the bulk air temperature of the exterior (24 °C). The latter can be explained as external forced convection occurring, and no radiation was supplied in the climate chamber. Nevertheless, in real conditions, buildings' outer walls are exposed to solar radiation, and their temperature can exceed ambient air by several units. For instance, Mazzali et al. (2013) evaluated three green walls separated by an open-air cavity from the cladding in a Mediterranean climate. It was found that during sunny days, the temperature difference monitored on the external wall's surface between the bare wall and the wall covered by the GW ranged from 12 °C to 20 °C. On the other hand, the difference reduced to values of 1 – 2 °C during cloudy days. A heat flux analysis was performed in which the surface heat transfer coefficient was the combination of the convective and radiative heat transfer coefficients, similar to the approach taken by Pastori et al. (2021). During high solar radiation values, a negative or outgoing flux was identified from the wall.

Freewan, Jaradat and Amaireh (2022) integrated and validated a thermal model for green walls on DesignBuilding. A bare wall scenario was considered to evaluate the temperature reduction provided by the green walls. It consisted of concrete (0.3 m) and bricks (0.1 m). The temperature reduction was measured at the exterior surface of the masonry. The model showed high agreement, and the green walls could decrease the masonry's external surface by 7 °C. Analogously, the thermal model integrated by Zhang, Zhang and Meng (2022) on EnergyPlus also compared a bare wall scenario against a green wall case based on the external surface temperature of the masonry. The bare wall was built according to the Chinese national standards

"Code for thermal design of civil engineering". The model could predict with a high agreement the external surface temperature of the masonry (RMSE = 0.53 °C).

The one-dimensional thermal model for green walls built by Scarpa, Mazzali and Peron (2014) considered a bare wall made of concrete (thickness = 0.40 m). It was validated with experimental measurements by considering the external surface wall's temperature. The model showed high correlation agreement and low values for RMSE, which agrees with our results. García et al. (2019) adapted and integrated two well-known green roof models with EnergyPlus to model heat and mass transfer through green walls and validated them under semiarid climate conditions. A high agreement between experimental and simulated data for the temperature of the foliage and substrate of the green wall was found (r > 0.80) and low RSME values (< 2.96 °C).

5.2 Green wall scenario

The temperature reduction offered by the GW-TPs can be seen as the summation of the reduction offered by insulation, evapotranspiration and air cavity mechanisms. Our work analyzes the temperature reduction offered by the GW-TP at the masonry's surface (T_w) against the bare wall case (**section 0**). This variable has been previously used to measure the cooling ability of green walls, as done by Arenghi, Perra and Caffi (2021) and Convertino, Vox and Schettini (2021). However, the hygrothermal model of GW implemented by Malys, Musy and Inard (2014) in SOLENE-microclimate focused on predicting the leaf and substrate temperature of the GW instead of the temperature reduction at the building wall's surface.

Figure 2 shows the predicted hygrothermal behavior, i.e., temperature profiles, and measured temperature, i.e., points for the four GW-TPs. The validation of the hygrothermal model for each GW-TP is likewise shown as in the bare wall case. A distinction was made between the scenario of no evapotranspiration (No-ET), i.e., no heat sinks, versus evapotranspiration (ET-adj). The latter included the vegetation's transpiration and the substrate's evaporation heat sink terms. The maximum air velocity obtained in the closed cavity for the four GW-TPs was 0.03 m s^{-1}, which is typical for natural convection. The bare wall case's temperature profile is also shown as the comparison basis.

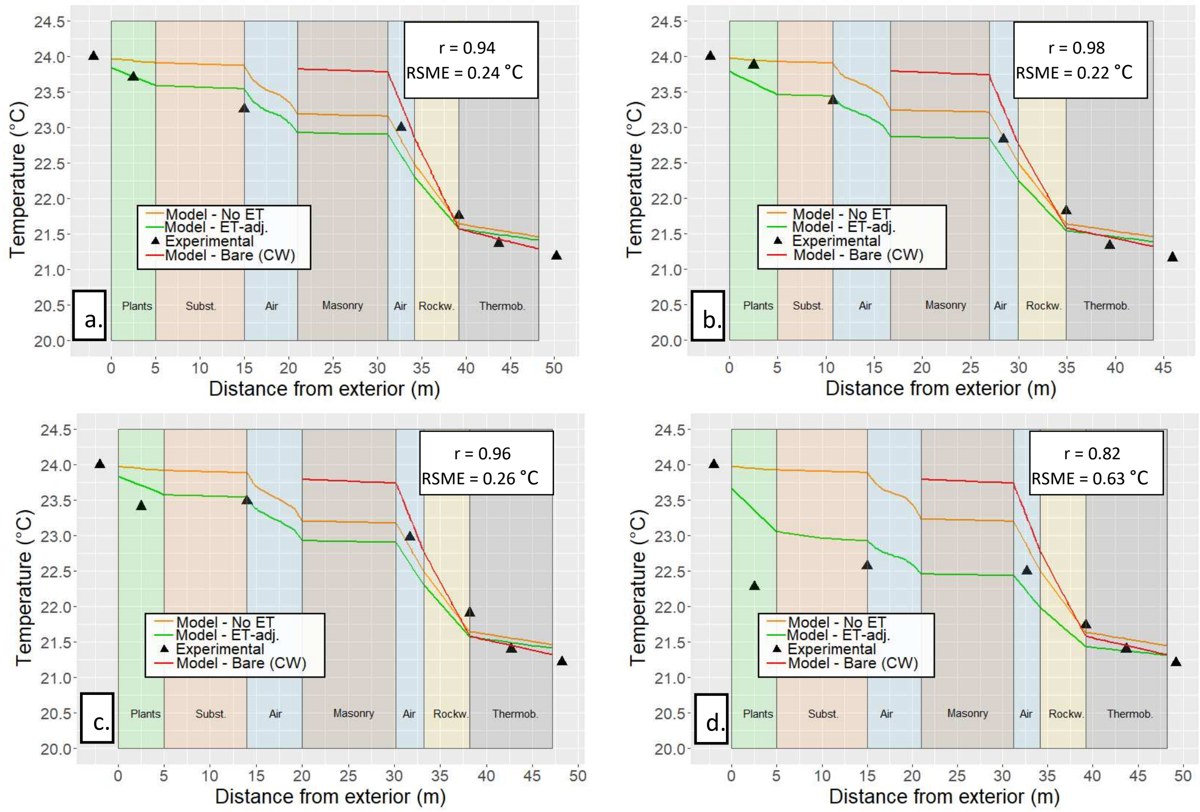

Figure 2. Simulated temperature (profiles) corresponding to different scenarios: (i) No evapotranspiration (No ET); (ii) Evapotranspiration (ET-adj) and experimental data (triangles) for the green wall case, i.e., green wall-test panel (GW-TP) mounted on the outer leaf of the insulated cavity wall (CW). No evapotranspiration (No ET) refers to the no use of heat sinks for evapotranspiration; evapotranspiration (ET-adj) is the scenario where heat sinks are enabled together with the insulation effect and the air cavity. The evaluated panels are (a) PANEL A; (b) PANEL B; (c) PANEL C; (d) PANEL D. Note: The first and the last triangle correspond to the setpoints in the climate chamber.

As seen in **Figure 2**, all GW-TPs produced a decreasing temperature profile from the exterior of the GW, i.e., vegetation's surface to the masonry's surface under both no-evapotranspiration (No-ET) and evapotranspiration (ET-adj) scenarios. The no-evapotranspiration scenario (No-ET) is a reference to analyze the extent of the temperature reduction, assuming that the GW-TPs provide only insulation; thus, the heat sink terms are not enabled. This scenario is important to comprehend the magnitude of the temperature decrease due to evapotranspiration (**Figure 3**). Notably, the temperature reduction was greater under evapotranspiration conditions (ET-adj), particularly for PANEL B and PANEL D, as their LAD values were the highest among the panels (PANEL B: $LAD = 0.8$; PANEL D: $LAD = 1.0$). Particulary, PANEL D had a thick substrate with a high water saturation ratio ($Sr = 0.4$) reaching the maximum temperature reduction amongst the GW-TPs (1.14 °C). Similarly, to our findings, Arenghi, Perra and Caffi, (2021) integrated a hygrothermal model in EnergyPlus and compared the surface temperature reduction when the GW was present against a concrete model. The study found that the reduction was up to 13°C due to the high thickness of the substrates that can subsequently host greater foliar density (LAD). Such results seem to outperform what we found in our work. Nevertheless, they considered the air cavity ventilated and solar radiation used as a boundary condition.

The major contribution of the air cavity to the temperature reduction of the masonry's surface (all GW-TPs) can be seen in **Figure 2**. This indicates that the thermal conductivity of air was not enhanced to a great extent by modeling natural convection in this section. More details about the air cavity contribution are given in **Figure 3. On the other hand,** the predicted temperature reduction at the substrate's rear (T_{bg}) of the GW-TPs was compared against experimental measurements (Fout! Verwijzingsbron niet gevonden.). The mean temperature reduction at the substrate's rear of the GW-TPs was 0.83 ± 0.41 SD °C compared to the model's output under evapotranspiration conditions (ET-adj) (0.57 ± 0.15 SD °C).

Table 4. Temperature reduction at the green wall-test panels' substrate rear (T_{gb}) due to the insulation and evapotranspiration effects. Note: This reduction is calculated based on the exterior temperature (24 °C).

Green Wall – Test Panel (GW-TP)	**Temperature reduction at the substrate's rear - T_{bg} (°C)**		
	Experimental	**Model**	**Correlation**
A	0.74	0.46	
B	0.62	0.56	
C	0.51	0.46	r = 0.92
D	1.43	0.78	

In this study, no experimental measurements were taken at the masonry's surface; thus, the GW-TPs contribution to reducing the masonry's surface temperature (T_w) under the different mechanisms is based on the model's output (**Figure 3**). The contribution of the air cavity to reducing the masonry's surface temperature (T_w) under evapotranspiration conditions was also calculated. On average, the GW-TPs decreased the masonry's surface temperature (model's output) by 0.97 ± 0.11 SD °C under the insulation + air cavity + evapotranspiration effects, i.e., blue bars in **Figure 3**. The temperature reduction attributed to the evapotranspiration effect under this scenario was 0.31 ± 0.20 SD °C (mean for all GW=TPs), representing, on average, 30% of the total temperature reduction at the masonry's surface. However, it reached 48% in the case of PANEL D. On the other hand, the air cavity accounted for 60.7 ± 0.09 % (on average) of the total temperature reduction at the masonry's surface

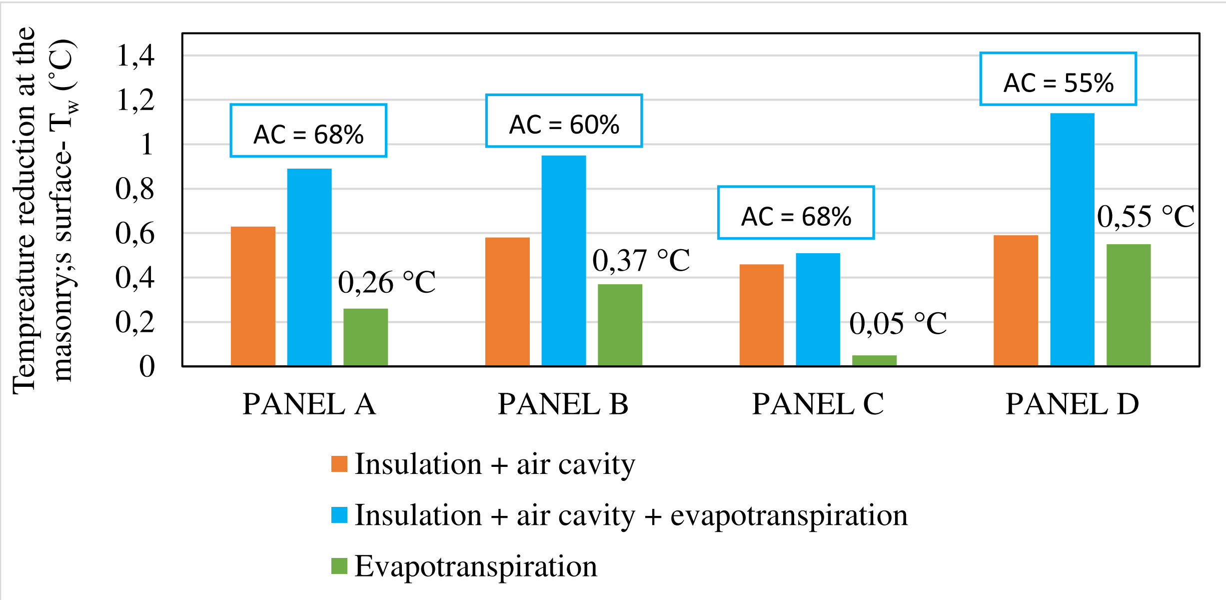

Figure 3. Contribution of the different mechanisms to the temperature reduction at the masonry's surface (T_w). AC: Air cavity contribution.

Generally, the building surface's temperature reduction found in this work is significantly lower than in previous work on green wall modeling. For instance, the thermal model integrated by Hoffmann et al. (2021) in the software package R simulated 36 scenarios of green cases vs. non-green cases (bare wall), and the exterior wall temperature reduction in all cases was up to 17

°C. Nevertheless, a high LAD value of 6.1 ± 0.5 was considered in all simulations, which is significantly greater than ours.

The work of F. Convertino, Vox and Schettini (2019) compared different mathematical methods to calculate the convective heat flux. The calculated convective flux was validated against experimental measurements from a green façade made of evergreen *Pandorea jasminoides* “Variegata” and a control wall (bare wall). In the experimental setup, the layers considered were external air, green layer, air gap (0.15 m), and external and internal surfaces of the building's external wall. The results showed that the empirical expressions efficiently predicted the convective flux in a green wall. However, the authors stated that convective exchanges were not dominant but solar radiation which directly influences evapotranspiration. Their experimental results showed that the reduction reached at the external surface temperature covered by the green façade (compared to the bare wall) from 10 AM to 5 PM was approximately 8 °C.

A mathematical model based on a heat balance and considering the shading, insulation, and evapotranspiration effect was integrated with EnergyPlus by Dahanayake and Chow (2017). Notably, the model considered solar radiation as a boundary condition from which the latent heat flux of evapotranspiration was calculated. The simulation showed that the GW could reduce building facades' surface temperature, especially during summer. As a result, a maximum reduction of 26 °C was reached in the exterior surface temperature of the façade.

Jim and He (2011) considered incident solar radiation as a boundary condition in a one-dimensional thermal model validated against experimental results. A shading coefficient was used to evaluate the shading performance of the green wall. The study showed that the shading effect of the green wall is dramatic (589.89 W m^{-2}, 39.65 °C) compared with the control wall (1168 W m^{-2}, 48.48 °C). Comparative, Kenai et al. (2021) focused on the radiative and convective exchange between green walls and the external environment. The external or outside surface temperature was likewise used to measure the reduction against a reference or bare house. It was found that under solar radiation peaks (813-850 W m^{-2}), the external surface temperature did not exceed 45 °C compared to 67 °C in the reference or bare house. Thus, when a thermal model considers solar radiation besides convection, the external surface of a bare wall (T_w) increases significantly. In contrast, a green wall will decrease that temperature as solar radiation promotes more evapotranspiration. Hence, we can hypothesize that the contribution of the GW-TPs in real scenarios might be greater than what we have found in this work.

A sole simulation was conducted in our software for PANEL 1 to verify the previous hypothesis. Solar radiation (500 W m^{-2}) was imposed as a boundary condition, i.e., heat flux, and the rest of the conditions were maintained constant. The vegetation albedo was set to 0.2 for the green wall scenario, and a value of 0.5 was for the masonry in the bare wall scenario. Our results showed that the masonry's surface temperature (T_w) of the bare wall scenario reached 47.2 °C. On the contrary, its value was reduced to 37.6 °C when PANEL 1 was present, i.e., green wall scenario. Hence, a temperature reduction of almost 10 °C was obtained when solar radiation was considered, which agrees with Mazzali et al., 2013 and Arenghi, Perra and Caffi (2021).

Figure 3 shows that the air cavity accounts for a major proportion of the temperature reduction at the masonry's surface (T_w), averaging 60% of this reduction when evapotranspiration conditions (ET-adj) were considered. The low thermal conductivity of air can and the low air velocity obtained by modeling natural convection (0.03 m s^{-1}) might explain the high-temperature reduction. Scarpa, Mazzali and Peron (2014) developed and validated a one-dimensional thermal model to compare a green wall mounted on a building wall with an open cavity vs. the same green wall with a closed air cavity. In the latter, natural convention was also modeled similarly to our work. The air cavity in both cases was maintained at 0.05 m thickness.

The study showed fewer temperature variations (external wall's surface) were obtained for the green wall with the enclosed cavity, especially during the winter.

5.3 Parametric study

Crucial parameters in a GW were varied, considering PANEL A to illustrate this impact on the masonry's surface temperature (T_w) (**Figure 4**). Leaf area density (LAD) has been recognized as the most sensitive parameter when calculating vegetation's transpiration. Nevertheless, appropriate techniques are lacking to measure this parameter (De Bock *et al.*, 2022). Therefore, leaf area density (LAD) was varied from 0.50 to 2.00 $m^2\ m^{-3}$ and the water saturation ratio (Sr) from 0.20 to 0.40 $m^3\ m^{-3}$. Parameter variation aims to identify the most effective combination to obtain the maximum temperature reduction at the masonry's surface.

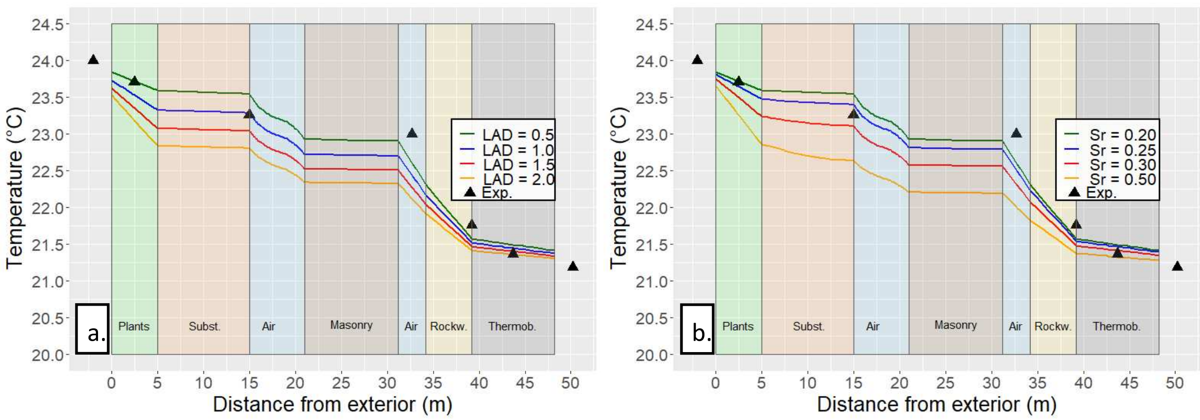

Figure 4. (a) Variation of leaf area density (LAD) and (b) substrate's water saturation (Sr) in PANEL A.

The parametric study showed that high LAD values translated into high-temperature reduction at the masonry's surface (T_w), as the evapotranspiration effect is enhanced by deducting more heat (**Figure 4,a**). For instance, a LAD value of 0.5 $m^2\ m^{-3}$ reduced the masonry's temperature (T_w) by 0.9 °C (compared to the bare wall), whereas a value of 2.0 $m^2\ m^{-3}$ only by 1.5 °C.

Arenghi, Perra and Caffi (2021) also performed a parametric study in their green wall's hygrothermal model varying LAD from 0.30 to 5.00 $m^2\ m^{-3}$ considering a GW operating under summer conditions. The latter LAD value produced an external surface temperature reduction of 2 °C compared to a LAD of 1 m^2 m^{-3}. Their parametric study also found that high LAD values produced a discrepancy between the simulated temperature profiles and the experimental measurements, which is congruent with our results in **Figure 4,a**.

Škerget, Tadeu and Almeida (2021) varied the LAD (1.5 – 4.5 m^3 m^{-3}) and the extinction coefficient to analyze the impact in their hygrothermal model for a green façade (thickness = 0.25 m) mounted on a single brick wall without insulation (thickness = 0.20 m). The extinction coefficient refers to the amount of solar radiation decreased by vegetation. The authors found that a dense canopy with a LAD value greater than 3 m^3 m^{-3} and an extinction coefficient greater than 0.7 effectively reduced the façade surface temperature.

We can hypothesize that the visually approached LAD value of PANEL A (0.5 m^2 m^{-3}) might have been the closest to the real value given that if used in the model, the simulated temperature profile matches the experimental data. Nevertheless, this value is conservative since LAD values from 2.0 to 3.0 m^2 m^{-3} have been used for hygrothermal models of GW. Therefore, additional techniques are required to verify the LAD values in the GW-TPs.

Figure 4,b describes that an increase in Sr led to a decrease in temperature at the masonry's temperature (T_w) since more heat is deducted from the heat balance, i.e., heat sink term. A Sr value of 0.2 m^3 m^{-3} decreased it by 0.9 °C, whereas a value of 0.25 only by 1.0 °C. We can also maintain the previous assumption of a Sr value of 0.2 m^3 m^{-3} in all GW-TPs (except for PANEL D, Sr = 0.4 m^3 m^{-3}), as this profile is the closest to the experimental data. It is sustained that variations in the water content of the substrate significantly contribute to temperature reduction.

Malys, Musy and Inard (2014) conducted a parametric study creating three samples varying the thickness of the vegetation (Sample 1= 0.40 m; Sample 2 = 0.35 m; Sample 3 = 0.40 m) and substate (Sample 1= 0.07 m; Sample 2 = 0.15 m; Sample 3 = 0.09 m). LAD and Sr values were kept constant (LAD = 2 m^3 m^{-3}; Sr = 4 m^3 m^{-3}). The study showed that more heat was transmitted to the building wall in Sample 1 and decreased in Sample 2 due to greater thickness. Finally, an increase in latent heat was obtained for Sample 3.

It is tough to compare the mere contribution of the substrate with other studies as substrates are highly varied in type, dimensions, and thermophysical properties. However, thicker and more continuous substrate layers are believed to lead to major temperature reductions as more evaporation occurs. Besides, as more thermal mass is present, substrates could host larger plant species which can subsequently contain greater LAD (Arenghi, Perra and Caffi, 2021).

6 Conclusions and future perspectives

This work evaluated a hygrothermal model for predicting the temperature reduction at the building wall's surface provided by green wall-test panels (GW-TPs). A 3D multiphysics model coupling heat and mass transfer and heat sink terms to account for the evapotranspiration effect was integrated into Comsol Multiphysics®. Such an approach offers unprecedented insights into the complex fluid dynamics and heat transfer mechanisms that govern the behavior of green walls and the application of more boundary conditions. The model was validated under steady-state conditions against experiments performed in a climate chamber with sensors placed at multiple positions across the entire wall composition, providing a much sounder base for validation. In addition, natural convection occurring in the enclosed air cavity was modeled, and its contribution was quantified. Finally, the masonry's surface temperature was paid special attention to compare the temperature reduction in a bare wall vs. a green wall scenario.

Our model predicted that under evapotranspiration conditions, including the insulation and air cavity effects, the four GW-TPs could decrease the masonry's surface temperature in the range of 0.89 to 1.14 ˚C (0.97 ± 0.11 SD ˚C) and a mean temperature reduction at the substrate's rear of 0.57 ± 0.15 SD °C. The temperature reduction attributed to the evapotranspiration effect under this scenario was 0.31 ± 0.20 SD °C (mean for all GW=TPs), which represents, on average, 30% of the total temperature reduction at the masonry's surface. The air cavity accounted for 60.7 ± 0.09 % (on average) at the same location. Such values are lower than previous hygrothermal models' predictions (> 10 ˚C), which can be explained as solar radiation was not replicated in our experiments nor used as a boundary condition in the model. However, we demonstrated that if considered, our model predicts a temperature reduction at the masonry's surface of almost 10 ˚C compared to the bare wall scenario. These results align with values reported in previous hygrothermal models.

The evaporation effect, which received special attention, was divided into the plant's transpiration and the substrate's evaporation. The former was expressed regarding biological parameters like leaf area density (LAD) and the latter in terms of the substrate's water content (Sr). Heat sink terms were applied in the model to represent the evapotranspiration effect which deducted heat from the global heat source.

Leaf area density (LAD) and the substrate's water saturation (Sr) directly impacted the ability of the GW to reduce the building's surface temperature. Higher values in both parameters were translated into higher temperature reduction values at the masonry's surface. Future work should employ innovative techniques to determine the real values of LAD that can be further used in the simulation. Hence, seeking their optimal combination to achieve maximum temperature reduction in future work is crucial.

7 Declaration of Competing Interest

The authors have no declarations of interest.

8 Acknowledgements

This project was funded by the "Flanders Innovation & Entrepreneurship Agency" under the project "TETRA WONDERWALLS FACILITATING GREEN FACADES."

9 References

Arenghi, A., Perra, C. and Caffi, M. (2021) ‘Simulating and comparing different vertical greenery systems grouped into categories using energyplus’, *Applied Sciences (Switzerland)*, 11(11). Available at: https://doi.org/10.3390/app11114802.

Arkebauer, T.J. (2005) *Leaf Radiative Properties and the Leaf Energy Budget*. Available at: https://digitalcommons.unl.edu/agronomyfacpub/693.

Ayata, T., Tabares-Velasco, P.C. and Srebric, J. (2011) ‘An investigation of sensible heat fluxes at a green roof in a laboratory setup’, *Building and Environment*, 46(9), pp. 1851–1861. Available at: https://doi.org/10.1016/j.buildenv.2011.03.006.

De Bock, A. *et al.* (2022) ‘A review on the leaf area index (LAI) in vertical greening systems’, *Building and Environment*, p. 109926. Available at: https://doi.org/10.1016/j.buildenv.2022.109926.

Cascione, V. *et al.* (2017) ‘Hygrothermal analysis of technical solutions for insulating the opaque building envelope’, in *Energy Procedia*. Elsevier Ltd, pp. 203–210. Available at: https://doi.org/10.1016/j.egypro.2017.08.141.

Convertino, Fabiana, Vox, G. and Schettini, E. (2019) ‘Convective heat transfer in green façade system’, *Biosystems Engineering*, 188, pp. 67–81. Available at: https://doi.org/10.1016/j.biosystemseng.2019.10.006.

Convertino, F., Vox, G. and Schettini, E. (2019) ‘Heat transfer mechanisms in vertical green systems and energy balance equations’, *International Journal of Design and Nature and Ecodynamics*, 14(1), pp. 7–18. Available at: https://doi.org/10.2495/DNE-V14-N1-7-18.

Convertino, F., Vox, G. and Schettini, E. (2021) ‘Evaluation of the cooling effect provided by a green façade as nature-based system for buildings’, *Building and Environment*, 203. Available at: https://doi.org/10.1016/j.buildenv.2021.108099.

Dahanayake, K.W.D.K.C. and Chow, C.L. (2017) ‘Studying the potential of energy saving through vertical greenery systems: Using EnergyPlus simulation program’, *Energy and Buildings*, 138, pp. 47–59. Available at: https://doi.org/10.1016/j.enbuild.2016.12.002.

Date, A.W. (2012) ‘Thermophysical and Transport Properties of Gases’, *Analytic Combustion*, pp. 325–333. Available at: https://doi.org/10.1017/cbo9780511976759.016.

Djedjig, R. *et al.* (2012) ‘Development and validation of a coupled heat and mass transfer model for green roofs’, *International Communications in Heat and Mass Transfer*, 39(6), pp. 752–761. Available at: https://doi.org/10.1016/j.icheatmasstransfer.2012.03.024.

Djedjig, R. *et al.* (2017) ‘Thermal effects of an innovative green wall on building energy performance’, *Mechanics and Industry*, 18(1). Available at: https://doi.org/10.1051/meca/2016015.

Djedjig, R., Bozonnet, E. and Belarbi, R. (2016) ‘Modeling green wall interactions with street canyons for building energy simulation in urban context’, *Urban Climate*, 16, pp. 75–85. Available at: https://doi.org/10.1016/j.uclim.2015.12.003.

Freewan, A.A., Jaradat, N.M. and Amaireh, I.A. (2022) ‘Optimizing Shading and Thermal Performances of Vertical Green Wall on Buildings in a Hot Arid Region’, *Buildings*, 12(2). Available at: https://doi.org/10.3390/buildings12020216.

García, M. *et al.* (2019) ‘Modelling and validation of two heat and mass transfer model of living walls and evaluation of their impact on the energy performance of a supermarket in a semiarid climate’, in *Building Simulation Conference Proceedings*. International Building Performance Simulation Association, pp. 488–493. Available at: https://doi.org/10.26868/25222708.2019.211051.

Hamdaoui, M.A. *et al.* (2021) ‘A review on physical and data-driven modeling of buildings hygrothermal behavior: Models, approaches and simulation tools’, *Energy and Buildings*, 251, p. 111343. Available at: https://doi.org/10.1016/j.enbuild.2021.111343.

Hoffmann, K.A. *et al.* (2021) ‘Modelling the cooling energy saving potential of facade greening in summer for a set of building typologies in mid-latitudes’, *Energy and Buildings*, 238. Available at: https://doi.org/10.1016/j.enbuild.2021.110816.

Jayalakshmy, M.S. and Philip, J. (2010) ‘Thermophysical properties of plant leaves and their influence on the environment temperature’, *International Journal of Thermophysics*, 31(11–12), pp. 2295–2304. Available at: https://doi.org/10.1007/s10765-010-0877-7.

Jim, C.Y. and He, H. (2011) ‘Estimating heat flux transmission of vertical greenery ecosystem’, *Ecological Engineering*, 37(8), pp. 1112–1122. Available at: https://doi.org/10.1016/J.ECOLENG.2011.02.005.

Kenai, M.A. *et al.* (2021) ‘Impact of green walls occultation on energy balance: Development of a TRNSYS model on a brick masonry house’, *Journal of Building Engineering*, 44(May). Available at: https://doi.org/10.1016/j.jobe.2021.102634.

Koch, K. *et al.* (2020) ‘Urban heat stress mitigation potential of green walls: A review’, *Urban Forestry and Urban Greening*, 55(August), p. 126843. Available at: https://doi.org/10.1016/j.ufug.2020.126843.

Lazzara, P. and Rana, G. (2010) *The crop coefficient (K c) values of the major crops grown under Mediterranean climate*. Available at: https://www.researchgate.net/profile/Kamel-Nagaz/post/Unusual_crop_coefficient_Kc_or_Kcb_of_specific_field_crops_in_arid_and_semi_arid_areas/attachment/5d01f3f43843b0b98256bab5/AS%3A769225572483072%401560409076192/download/The+crop+coefficient+%28Kc%29+values+of+the+major+crops+grown+under+Mediterranean.pdf (Accessed: 21 December 2022).

Malys, L., Musy, M. and Inard, C. (2014) ‘A hydrothermal model to assess the impact of green walls on urban microclimate and building energy consumption’, *Building and Environment*, 73, pp. 187–197. Available at: https://doi.org/10.1016/j.buildenv.2013.12.012.

Mazzali, U. *et al.* (2013) ‘Experimental investigation on the energy performance of Living Walls in a temperate climate’, *Building and Environment*, 64, pp. 57–66. Available at: https://doi.org/10.1016/j.buildenv.2013.03.005.

Pastori, S. *et al.* (2021) ‘Energy performance evaluation of a ventilated façade system through cfd modeling and comparison with international standards’, *Energies*, 14(1). Available at: https://doi.org/10.3390/en14010193.

ROCKWOOL (2022) *Rockfit Mono Isolatie voor spouwmuren*.

Sailor, D.J. (2008) ‘A green roof model for building energy simulation programs’, *Energy and Buildings*, 40(8), pp. 1466–1478. Available at: https://doi.org/10.1016/j.enbuild.2008.02.001.

Scarpa, M., Mazzali, U. and Peron, F. (2014) ‘Modeling the energy performance of living walls: Validation against field measurements in temperate climate’, *Energy and Buildings*, 79, pp. 155–163. Available at: https://doi.org/10.1016/j.enbuild.2014.04.014.

Škerget, L., Tadeu, A. and Almeida, J. (2021) ‘Article unsteady coupled moisture and heat energy transport through an exterior wall covered with vegetation’, *Energies*, 14(15), pp. 1–26. Available at: https://doi.org/10.3390/en14154422.

Šuklje, T., Medved, S. and Arkar, C. (2016) ‘On detailed thermal response modeling of vertical greenery systems as cooling measure for buildings and cities in summer conditions’, *Energy*, 115, pp. 1055–1068. Available at: https://doi.org/10.1016/j.energy.2016.08.095.

Widiastuti, R. *et al.* (2022) ‘Thermal insulation effect of green façades based on calculation of heat transfer and long wave infrared radiative exchange’, *Measurement: Journal of the International Measurement Confederation*, 188. Available at: https://doi.org/10.1016/j.measurement.2021.110555.

Wienerberger (2021a) *Forum Branco Handvorm / Moulée-main*. Available at: www.wienerberger.be.

Wienerberger (2021b) *POROTHERM Thermobrick 10N*. Available at: https://ce.wienerberger.be.

van de Wouw, P.M.F., Ros, E.J.M. and Brouwers, H.J.H. (2017) ‘Precipitation collection and evapo(transpi)ration of living wall systems: A comparative study between a panel system and a planter box system’, *Building and Environment*, 126, pp. 221–237. Available at: https://doi.org/10.1016/j.buildenv.2017.10.002.

Zhang, Y., Zhang, L. and Meng, Q. (2022) ‘Dynamic heat transfer model of vertical green façades and its co-simulation with a building energy modelling program in hot-summer/warm-winter zones’, *Journal of Building Engineering*, 58(July), p. 105008. Available at: https://doi.org/10.1016/j.jobe.2022.105008.

Appendix A

Green Wall-Test Panels Description

Each GW-TP dimension was 0.52 m (height) x 0.61 m (width) with variable thickness according to the substrate. The GW-TPs were mounted on the outer leaf of an insulated cavity wall (CW) that serves as a control representing a building wall. The latter consisted of (from outer to inner side) masonry (0.102 m), air gap (0.03 m), rockwool (insulation) (0.05 m), and Thermobrick (0.09 m).

Figure A.1. Green wall-test panels (GW-TPs) assessed in the climate chamber. (a) PANEL A; (b) PANEL B; (c) PANEL C; (d) PANEL D.

Appendix B

Climate Chamber

The chamber was operated by the Energy and Materials in Infrastructure and Buildings (EMIB) Research Group of the Department of Applied Engineering, University of Antwerp.

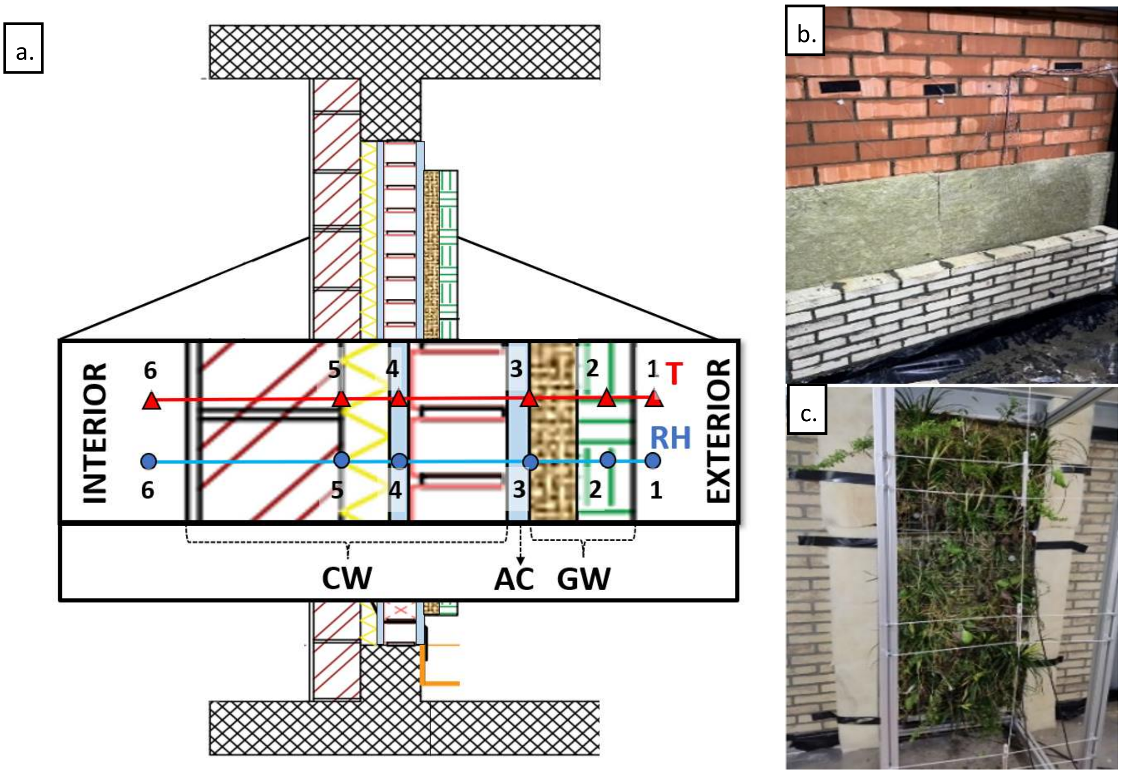

Figure B.1. (a) Side view of the climate chamber with the green wall (GW) compartment, which is separated from the insulated cavity wall (CW) by an air cavity (AC). The exterior of the CW is the masonry's surface, whereas its interior corresponds to the Thermobrick surface. Six sensors to measure temperature (red triangles), i.e., T1 – T6, and relative humidity (blue points) RH1 – RH6, are purposedly located across the setup (from the exterior to the interior of the setup), each placed in the following order: (1) exterior room; (2) middle of the vegetation; (3) rear of the substrate; (4) middle of the inner air cavity between masonry and Rockwool; (5) backside of the Rockwool; (6) interior room. (b) Photograph of the different materials that constitute the insulated cavity wall (CW). (c) Photograph of the green wall test panels (GW-TP) evaluated in the climate chamber, mounted on the exterior or outer leaf of the insulated air cavity wall (CW).

Appendix C

Thermophysical properties.

Table C.1. Thermophysical properties of the layers constituting the setup evaluated in the present work.

Section	Layer	Thermal conductivity (k)	Specific heat capacity (C_p)	Density (ρ)	Vapor resistance factor (μ)	Reference
		W m^{-1} K^{-1}	*J kg^{-1} K^{-1}*	*kg m^{-3}*	*(-)*	
Green wall-test panel (GW)	Vegetation	0.5	2252	656	1	(Jayalakshmy and Philip, 2010)
	Substrate	1.5	2085	1500	1.4	(Arenghi, Perra and Caffi, 2021).
Air cavity	Air	0.025	1006	1.23	1	(Date, 2012)
Insulated cavity wall (CW)	Masonry	1.61	800	1800	13	(Wienerberger, 2021a)
	Air	0.025	1006	1.23	1	
	Rockwool	0.035	1030	35	1.4	(ROCKWOOL, 2022)
	Thermobrick	0.29	1000	100	13	(Wienerberger, 2021b)